JACS
JOURNAL OF THE AMERICAN CHEMICAL SOCIETY
Communication
pubs.acs.org/JACS

Chemical Excision of Tetrahedral $FeSe_2$ Chains from the Superconductor FeSe: Synthesis, Crystal Structure, and Magnetism of $Fe_3Se_4(en)_2$

Chongin Pak, Saeed Kamali, Joyce Pham, Kathleen Lee, Joshua T. Greenfield, and Kirill Kovnir*

Department of Chemistry, University of California, Davis, One Shields Avenue, Davis, California 95616, United States

Supporting Information

ABSTRACT: Fragments of the superconducting FeSe layer, $FeSe_2$ tetrahedral chains, were stabilized in the crystal structure of a new mixed-valent compound $Fe_3Se_4(en)_2$ (en = ethylenediamine) synthesized from elemental Fe and Se. The $FeSe_2$ chains are separated from each other by means of $Fe(en)_2$ linkers. Mössbauer spectroscopy and magnetometry reveal strong magnetic interactions within the $FeSe_2$ chains which result in antiferromagnetic ordering below 170 K. According to DFT calculations, anisotropic transport and magnetic properties are expected for $Fe_3Se_4(en)_2$. This compound offers a unique way to manipulate the properties of the Fe−Se infinite fragments by varying the topology and charge of the Fe-amino linkers.

The chemistry of the recently discovered Fe-based superconductors is far from being fully explored.[1] The main structural blocks of Fe-based superconductors are FeX square layers (X = pnicogen or chalcogen) with a PbO-like structure. Each layer is formed from linear FeX_2 tetrahedral chains sharing all vertices (Figure 1A). To understand the electronic and magnetic interactions in superconductors it is preferable to study a single building block, i.e. an isolated FeX layer or FeX_2 chain.[2] To compare the calculated results with experimental observations it is necessary to develop "chemical scissors" that are able to excise a fragment of the superconducting phase. Additionally, it is desirable that the "chemical scissors" do not alter bonding within the cut fragment; i.e., the cutting reactant is only weakly coordinated to the FeX moiety. Here, we demonstrate how tetrahedral $FeSe_2$ chains (Figure 1B) can be isolated from each other by means of $[Fe(en)_2]^{2+}$ inorganic complexes, en = ethylenediamine. We report the synthesis, crystal structure, and magnetic properties of the new compound $Fe_3Se_4(en)_2$.

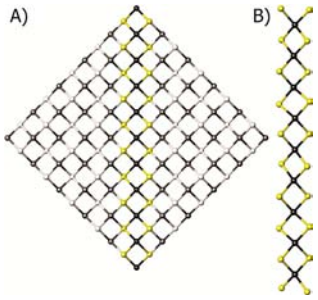

Figure 1. (A) Superconducting FeSe layer. Fe: black; Se: white/yellow. The $FeSe_2$ chain is emphasized in color. (B) Tetrahedral $FeSe_2$ chain in the crystal structure of $Fe_3Se_4(en)_2$.

$Fe_3Se_4(en)_2$ was synthesized through a solvothermal method from elemental Fe and Se (see Supporting Information for synthetic and characterization details). A small admixture of binary $FeSe_2$[3] was often present in the samples. The samples were characterized by conventional and high resolution synchrotron X-ray powder diffraction (XRD) (Figures SI 1 and SI 2). Single crystal X-ray diffraction refinement (Table SI 1) was performed in the space group $C2/c$ (No. 15).[4a] Elemental analysis of selected single crystals confirmed the presence of Fe and Se in 42(2)%:58(2)% ratio which is in agreement with calculated ratio of 43%:57%. Density functional theory calculations were performed using a full potential all-electron local orbital code FPLO 7.00−28 within the local density approximation.[4b]

^{57}Fe Mössbauer spectra were collected using a conventional constant acceleration spectrometer. Additionally, binary compound $FeSe_2$ was measured under the same conditions as $Fe_3Se_4(en)_2$. The parameters from the fittings are summarized in Table SI 2. The $Fe_3Se_4(en)_2$ sample used for Mössbauer spectroscopy contained 6 mol % of $FeSe_2$. To ensure that the contribution from the impurity was correctly described an impurity-enriched sample (18% $FeSe_2$) and a sample of pure $FeSe_2$ were measured under identical conditions (Figure SI 5, Table SI 3). $FeSe_2$ remains nonmagnetic above 80 K. All subsequent discussions pertain to signals from $Fe_3Se_4(en)_2$ after subtraction of the $FeSe_2$ signal.

Solvothermal syntheses of anisotropic selenides starting from soluble metal-containing precursors are well developed.[5] Most of the reported syntheses require hazardous and air-/moisture-sensitive reducing reagents or starting materials (e.g., $NaBH_4$ or $TiCl_4$). We have developed a simple route, which utilizes elemental Fe and Se (eq 1):

$$3Fe + 4Se + 2en \rightarrow Fe_3Se_4(en)_2 \quad (1)$$

This synthesis occurs at a low temperature (473 K) under aerobic conditions. Thus, no glovebox or Schlenk line is necessary. The addition of the mineralizer (NH_4Cl) is essential to increase the solubility of Fe and overall yield of the reaction. A similar increase in metal solubility was observed in our earlier studies synthesizing tin arsenide.[6] NH_4Cl precipitates can be

Received: October 25, 2013
Published: December 3, 2013

   dx.doi.org/10.1021/ja410820u | J. Am. Chem. Soc. 2013, 135, 19111−19114

effectively washed out of the product with water or ethanol. $Fe_3Se_4(en)_2$ appears to be stable against treatment with water and ethanol; yet, it decomposes in dilute acidic solutions. $AFeSe_2$ (A = K, Rb, Cs) containing structural fragments similar to $Fe_3Se_4(en)_2$ were synthesized using a high temperature (1000 K) stream of highly toxic H_2Se gas.[7a] Our reported synthetic method is much more attractive due to its simplicity and the possibilities of fine-tuning the metal−amino complex, which will result in new related materials.

The crystal structure of $Fe_3Se_4(en)_2$ consists of two main structural units, one-dimensional $FeSe_2$ infinite chains, and $Fe(en)_2$ fragments (Figure 2A and 2B). The $FeSe_2$ chains are formed by $FeSe_4$ tetrahedra, which share opposite edges. A similar structural fragment is present in the superconducting tetragonal FeSe (Figure 1) where $FeSe_2$ chains are condensed together by sharing two additional edges, forming square layers with the overall composition FeSe.[1c] In the crystal structure of $Fe_3Se_4(en)_2$ half of the Se atoms from different $FeSe_2$ chains are connected via additional Fe atoms, labeled Fe2. The Fe2−Se bond (2.70 Å) is significantly longer than the Fe1−Se bond within the tetrahedral chains (2.35−2.40 Å). The atomic coordination of Fe2 atoms is completed by four coplanar N atoms from two ethylenediamine molecules (Figure 2B). Tetrahedral $Fe1Se_2$ chains run along the [001] direction (Figure 2C and 2D). Se atoms that are not bound to Fe2 atoms are additionally coordinated by one H atom from the ethylenediamine moiety at a distance of 2.56 Å. Thus, every Se atom has a 2 + 1 coordination. The average Fe2−N distance of 2.18 Å is typical for the high spin state of Fe^{2+}.[8] Isolated $FeSe_2$ chains were stabilized only by the presence of high concentrations of alkali metals cations in $AFeSe_2$ (A = K, Rb, Cs) compounds.[7a] In $AFeSe_2$ the tetrahedral chains are slightly distorted from ideal $p4_2/mmc$ rod group symmetry. For example, in $RbFeSe_2$ the Fe−Se distances are 2.383 and 2.386 Å and the angles ∠Se−Fe−Se (107.1°−111.5°) are close to the ideal tetrahedral angle of 109.5°.[7a] Theoretical investigations of the sulfur analogs by Silvestre and Hoffmann predict little distortion of the $[FeS_2]^{1-}$ tetrahedral chains based solely on electronic factors.[7b] Strong Peierls distortion was predicted for the $[FeS_2]^{1.5-}$ reduced chains, which was indeed observed in $A_3Fe_2X_4$ (X = S, Se).[7c,d] In $Fe_3Se_4(en)_2$ the tetrahedral chains bear a −1 formal negative charge (see the Mössbauer section below). However, they exhibit a much stronger deviation from the ideal $p4_2/mmc$ rod group symmetry with Fe−Se distances varying from 2.352 to 2.397 Å and angles ∠Se−Fe−Se from 103.8° to 117.1°. These distortions are caused by chain−cation interactions. In $AFeSe_2$ each Se atom is additionally coordinated by four A^+ cations at distances >3.5 Å.[7a] In $Fe_3Se_4(en)_2$ the $FeSe_2$ chains are further apart from each other compared to $AFeSe_2$. Nevertheless, in $Fe_3Se_4(en)_2$ each Se atom has one short neighbor outside the chain: either Fe2 atoms at distance of 2.70 Å or a H atom at a distance of 2.56 Å. Such secondary Se−cation interactions introduce significant distortions to the tetrahedral chain, which are unexpected from a solely electronic point of view.

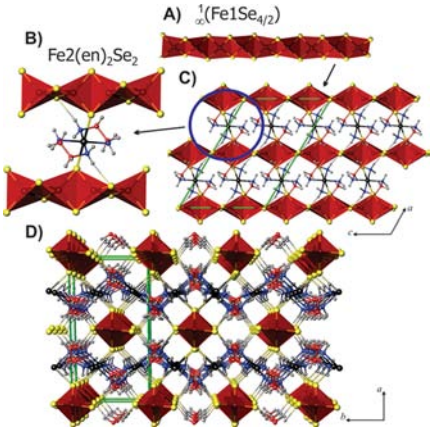

Figure 2. Crystal structure of $Fe_3Se_4(en)_2$: (A) tetrahedral $Fe1Se_2$ chain; (B) $Fe2(en)_2Se_2$ fragment connecting two tetrahedral chains; (C and D) general views along the [010] and [001] directions. Long Se−Fe and Se−H bonds are shown using dashed lines. The unit cell: green; Fe: black; Se: yellow; N: blue; C: red; H: gray; $FeSe_4$ tetrahedra: red.

High-resolution XRD confirmed the structure established by single-crystal diffraction (Figure SI 2, Table SI 1). Comparison of the structural data obtained from single crystal and powder XRD experiments performed at 90, 100, and 295 K reveals the absence of any structural transition. Fe2−N and Fe1−Se distances remain almost unchanged, and the structural shrinkage upon cooling occurs mainly due to shortening of the long Fe2−Se bonds (Tables SI 1 and SI 4).

The role of the ethylenediamine ligand in $Fe_3Se_4(en)_2$ is to coordinate Fe2 atoms connecting the $FeSe_2$ chains. This differentiates the title compound from metal−organic frameworks where coordinating ligands provide connectivity between metal centers and dictate the topology of the framework.[9] $Fe_3Se_4(en)_2$ also stands apart from the majority of solvothermally synthesized metal chalcogenides. For most of them the amine molecule either connects two inorganic fragments (e.g., MnSe slabs connected by en)[5d] or coordinates to the inorganic fragments (en coordinated to TiX_2 chains, X = S, Se).[5a,b] In the crystal structure of $Fe_3Se_4(en)_2$ two independent subsystems can be identified: $FeSe_2$ chains and $Fe(en)_2$ complexes. Each subsystem has different contributions to the magnetism and electronic structure as shown below.

$Fe_3Se_4(en)_2$ is paramagnetic at 300 K (Figure 3). No satisfactory Curie−Weiss fitting can be achieved involving a temperature independent contribution, χ_{TIP} (Table SI 5). Fixing $\chi_{TIP} = 0$ results in a reasonable fit with the asymptotic Curie temperature, $\theta = -105(8)$ K, which indicates antiferromagnetic (AFM) nearest-neighbor interactions (Table SI 5, Figure SI 6). The χT value at 300 K is only 4.2 emu·K·mol^{-1}, while from Curie−Weiss fitting it is 5.6(2) emu·K·mol^{-1}. Such low χT values indicate that the Fe states may differ from high spin Fe^{2+} ($S = 2$) and Fe^{3+} ($S = 5/2$). To further clarify the oxidation and spin states of Fe atoms, Mössbauer spectroscopy was applied. The room temperature spectrum for $Fe_3Se_4(en)_2$ was fitted with two doublets, Q_1 and Q_2, with a 2:1 intensity ratio (Figure 4A, Table SI 2). Q_1, with a low chemical shift (0.27 mm/s) and quadrupole

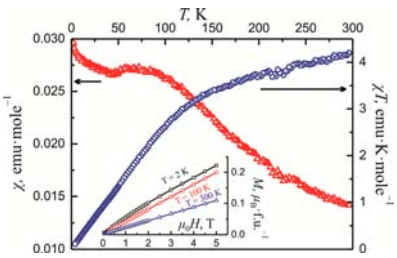

Figure 3. Temperature dependence of magnetic susceptibility χ (red △) and χT (blue ○) for $Fe_3Se_4(en)_2$ in the applied field of 3 mT. Inset: isothermal field dependence of the magnetization.

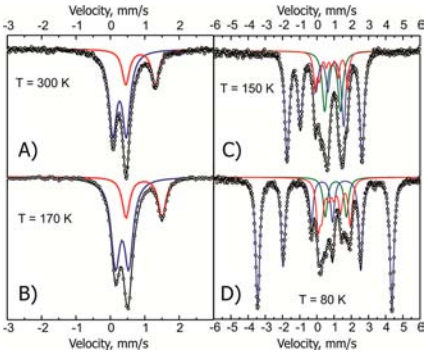

Figure 4. Mössbauer spectra for $Fe_3Se_4(en)_2$ collected at different temperatures. Experimental data: black circles; calculated spectrum: black line; Fe^{3+}: blue; Fe^{2+}: red and green.

splitting (0.39 mm/s), corresponds to tetrahedral Fe^{3+}. The chemical shift of the Fe^{3+} is slightly smaller than the reported chemical shift for Fe^{3+} atoms in $AFeSe_2$.[7e] Q_2, with a high chemical shift (0.88 mm/s) and high quadrupole splitting (0.86 mm/s), corresponds to a high-spin Fe^{2+}. The high value of the chemical shift unambiguously indicates an $S = 2$ spin state, despite the 4/*mmm* distortion of the Fe^{2+} environment.[10] Thus, $Fe_3Se_4(en)_2$ is a mixed valent compound containing well separated Fe^{3+} and Fe^{2+} sublattices. In the crystal structure the ratio of Fe1/Fe2 is 2:1. Assuming that en is a neutral ligand, the formula of the compound can be written as $(Fe^{2+})(en^0)_2(Fe^{3+})_2(Se^{2-})_4$. Therefore, Fe atoms in the tetrahedral chains are Fe^{3+}, while Fe atoms coordinated to en are Fe^{2+}, differentiating the title compound from the binary FeSe superconducting phase in which all iron atoms are Fe^{2+}.[1c,11] The bond-valence sum calculations support the Mössbauer assignments giving +3.1 and +1.9 oxidation states for tetrahedral and octahedral Fe atoms, respectively.[12]

Fe^{3+} in a strongly distorted tetrahedral environment with a +0.27 mm/s Mössbauer chemical shift may have three spin states: $S = 1/2$, 3/2, and 5/2.[7e,10] According to neutron diffraction data, the local crystal field, and extended band structure calculations, Fe^{3+} in $AFeSe_2$ exhibits an intermediate spin state between $S = 3/2$ and 1/2.[7] For $Fe_3Se_4(en)_2$, χT values in the range 3.75−6.75 emu·K·mol^{-1} are expected assuming $S = 2$ for Fe^{2+} and $S = 1/2$ or 3/2 for Fe^{3+}. The observed χT values are in this range indicating mixed spin states for Fe^{3+}. A gradual decrease of the χT with temperature indicates the presence of AFM coupling between Fe atoms, which is supported by the investigation of the isothermal field dependence of magnetization (Figure 3 inset). The magnetic moment at rt at the highest applied field of 5 T was only 0.1 μ_B·f.u.$^{-1}$.

Upon cooling an AFM transition due to the interaction between the chains is observed starting at ∼150 K (Figure 3). The AFM nature of the transition is emphasized by a significant decrease of χT with decreasing temperature and supported by the low temperature field dependences of magnetization (Figure 3 inset). Mössbauer spectroscopy was used to trace the AFM ordering. The spectrum collected at 170 K is similar to the rt one taking into account the second-order Doppler effect, which is reflected in the increase in chemical shifts with decreasing temperature (Figure 4B). At 150 K, the Fe^{3+} component, Q_1, is completely transformed to a magnetic sextet with a hyperfine field of 13.5 T (blue line in Figure 4C). This is comparable with the hyperfine field in $AFeSe_2$.[7e] The Fe^{2+} component consists of two signals: a nonmagnetic doublet (green line in Figure 4C) and a magnetically split sextet (red line in Figure 4C). The latter component exhibits a significantly smaller hyperfine field of 5.9 T. Similar behavior was observed for $BaFe_2Se_3$, where double-tetrahedral chains are present.[13] Further cooling to 80 K decreased the intensity of the nonmagnetic part of Fe^{2+} and increased the intensity of the Fe^{2+} sextet (Figure 4D, Table SI 2). Additionally, the hyperfine field for both observed sextets increased. Mössbauer signals from $Fe_3Se_4(en)_2$ collected at 10 K are similar to those observed at 80 K with a small increase of hyperfine field to 6.6 T for the magnetic Fe^{2+} component (Figure SI 4, Table SI 2). At 10 K the hyperfine field for Fe^{3+} is 25.7 T which is expected for $S = 3/2$[7e] and lower than typical values of ∼50 T for $S = 5/2$.[10]

Simple molecular orbital calculations based on local structure may explain the low spin state of Fe^{3+}, but will also predict the lower spin state of $S = 1$ for Fe^{2+} in $Fe(en)_2Se_2$. This contradicts the Mössbauer data, since for Fe^{2+} with $S = 1$ a significantly smaller chemical shift (<0.6 mm/s) is expected.[10] Silvestre and Hoffmann have performed a detailed analysis of local and extended bonding in $[FeS_2]^{1-}$ tetrahedral chains and have shown that simple local MO analysis is not sufficient to explain the magnetic and electronic properties. We performed nonmagnetic quantum mechanical calculations to qualitatively estimate the electronic structure of $Fe_3Se_4(en)_2$ (Figure 5). The title compound exhibits a high peak in the electronic density of states (DOS) in the vicinity of the Fermi level. Contrary to the simple valence description $(Fe^{2+})(en^0)_2(Fe^{3+})_2(Se^{2-})_4$, orbital overlap leads to the closing of the band gap.[14] As expected from the crystal structure, the electronic structure of $Fe_3Se_4(en)_2$ is strongly anisotropic. In the band diagram there are no bands crossing the Fermi level in the Γ−X and Z−L directions (Figure SI 7) of the Brillouin zone. Ethylenediamine and selenium have minor contributions to the states near the Fermi level. Our calculations indicate that magnetic ordering is expected for Fe^{3+} atoms but not for Fe^{2+}. The strongest contribution to the states in the vicinity of the Fermi level is from the 3d orbitals of Fe^{3+} atoms, while the 3d orbitals of Fe^{2+} are located below the Fermi level (Figure 5B). In itinerant magnets, the presence of a high DOS peak in the vicinity of the Fermi level is a prerequisite for magnetic ordering.[15] This explains the results of Mössbauer spectroscopy. Fe^{3+} atoms indeed exhibit magnetic ordering inside the tetrahedral chains resulting in a strong internal magnetic field and the high hyperfine splitting of the Mössbauer spectra. In turn, Fe^{2+} atoms do not exhibit magnetic ordering. The small hyperfine splitting is induced by the magnetic field of $FeSe_2$ chains. The absence of the sharp AFM peak in the magnetic susceptibility temperature dependence indicates that three-dimensional ordering of the magnetic moments of the chains is not perfect. Thus two situations are possible: $Fe^{3+}(\uparrow)Se-Fe^{2+}-SeFe^{3+}(\downarrow)$ and $Fe^{3+}(\uparrow)Se-Fe^{2+}-SeFe^{3+}(\uparrow)$.

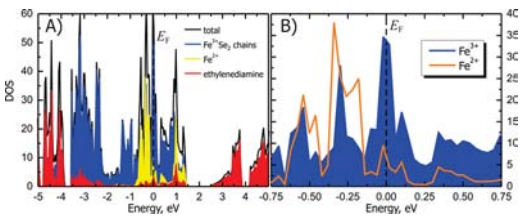

Figure 5. Non-spin-polarized DOS for $Fe_3Se_4(en)_2$.(A) Contributions from $Fe^{3+}Se_2$ chains, en, and Fe^{2+} are shown. (B) Contributions of Fe^{3+} (blue) and Fe^{2+} (orange line) atoms are compared.

The former results in the cancelation of the induced magnetic field on Fe^{2+} and the appearance of the nonmagnetic doublet for Fe^{2+}, while the latter leads to the emergence of the magnetically induced sextet with a small hyperfine field.

Our magnetic, Mössbauer, and theoretical investigations of $Fe_3Se_4(en)_2$ indicate that within the $FeSe_2$ chains there is a strong antiferromagnetic interaction, while the interactions between the $FeSe_2$ chains are weaker. Upon cooling, the interactions between the chains strengthen resulting in the attenuation of the nonmagnetic Fe^{2+} component in the Mössbauer spectra. Yet, one-fourth of the Fe^{2+} atoms remains nonmagnetic at 10 K, indicating that complete 3-D antiferromagnetic ordering of the Fe^{3+} magnetic moments has not been achieved even at temperatures as low as 10 K.

A new crystal structure with tetrahedral $FeSe_2$ chains was synthesized from the simplest starting materials, elemental Fe and Se. $Fe_3Se_4(en)_2$ exhibits AFM ordering within the chains. This compound offers a unique way to study magnetic and electronic interactions in an isolated fragment of the superconductor FeSe. In condensed matter physics, the application of hydrostatic pressure is a common way to modify properties of a material.[16] $Fe_3Se_4(en)_2$ offers an alternative chemical method to introduce internal pressure. The "chemical pressure" can be achieved by varying the nature of the amine ligand, i.e. the length of the carbon chain or number of chelating amino groups. A variety of interesting magnetic and superconducting properties may arise from compounds with tunable, antiferromagnetically coupled tetrahedral $FeSe_2$ chains. Investigations to study the synthesis, structure, and properties of new compounds with similar chains and different amino ligands are currently underway.

■ ASSOCIATED CONTENT

Supporting Information

Crystallographic files, additional X-ray and Mössbauer tables and figures. This material is available free of charge via the Internet at http://pubs.acs.org.

■ AUTHOR INFORMATION

Corresponding Author

kkovnir@ucdavis.edu

Notes

The authors declare no competing financial interest.

■ ACKNOWLEDGMENTS

We thank M. Shatruk (FSU) for the fruitful discussions, A.V. Olenev (UC Davis) for help with single crystal X-ray diffraction experiments, and M. Suchomel (APS) for assistance with the collection of the high-resolution XRD pattern. C.P. acknowledges the UC Davis Provost Undergraduate Fellowship. UC Davis is gratefully acknowledged for financial support. The Mössbauer facility was supported by NIH Grant No. 1S10RR023656-01A1. Use of the Advanced Photon Source at Argonne National Laboratory was supported by the U.S. Department of Energy, Office of Science, Office of Basic Energy Sciences, under Contract No. DE-AC02-06CH11357.

■ REFERENCES

(1) (a) Kamihara, Y.; Hiramatsu, H.; Hirano, M.; Kawamura, R.; Yanagi, H.; Kamiya, T.; Hosono, H. *J. Am. Chem. Soc.* **2008**, *130*, 3296. (b) Rotter, M.; Tegel, M.; Johrendt, D. *Phys. Rev. Lett.* **2008**, *101*, 107006. (c) Hsu, F. C.; Luo, J. Y.; Yeh, K. W.; Chen, T. K.; Huang, T. W.; Wu, P. M.; Lee, Y. C.; Huang, Y. L.; Chu, Y. Y.; Yan, D. C.; Wu, M. K. *Proc. Natl. Acad. Sci. U.S.A.* **2008**, *105*, 14262. (d) Johnston, D. C. *Adv. Phys.* **2010**, *59*, 803. (e) Mazin, I. I. *Nature* **2010**, *464*, 183. (f) Canfiled, P. C. *Nat. Mater.* **2011**, *10*, 259. (g) Burrard-Lucas, M.; Free, D. G.; Sedlmaier, S. J.; Wright, J. D.; Cassidy, S. J.; Hara, Y.; Corkett, A. J.; Lancaster, T.; Baker, P. J.; Blundell, S. J.; Clarke, S. J. *Nat. Mater.* **2013**, *12*, 15. (h) He, S. L.; He, J. F.; Zhang, W. H.; Zhao, L.; Liu, D. F.; Liu, X.; Mou, D. X.; Ou, Y. B.; Wang, Q. Y.; Li, Z.; Wang, L. L.; Peng, Y. Y.; Liu, Y.; Chen, C. Y.; Yu, L.; Liu, G. D.; Dong, X. L.; Zhang, J.; Chen, C. T.; Xu, Z. Y.; Chen, X.; Ma, X.; Xue, Q. K.; Zhou, X. J. *Nat. Mater.* **2013**, *12*, 605.

(2) Andersen, O. K.; Boeri, L. *Ann. Phys.* **2011**, *523*, 8.

(3) Kjekshus, A.; Rakke, T.; Andresen, A. F. *Acta Chem. Scand.* **1978**, *A28*, 996.

(4) (a) Sheldrick, G. M. *Acta Crystallogr.* **2008**, *A64*, 112. (b) Koepernik, K.; Eschrig, H. *Phys. Rev. B* **1999**, *59*, 1743.

(5) (a) Liu, Y. H.; Porter, S. H.; Goldberger, J. E. *J. Am. Chem. Soc.* **2012**, *134*, 5044. (b) Li, T.; Liu, Y. H.; Porter, S. H.; Goldberger, J. E. *Chem. Mater.* **2013**, *25*, 1477. (c) Menezes, P. W.; Fässler, T. F. *Z. Naturforsch.* **2012**, *67B*, 651. (d) Huang, X. Y.; Heulings, H. R.; Le, V.; Li, J. *Chem. Mater.* **2001**, *13*, 3754. (e) Li, J.; Chen, Z.; Wang, R. J.; Proserpio, D. M. *Coord. Chem. Rev.* **1999**, *190−192*, 707. (f) Nitsche, F.; Goltz, T.; Klauss, H.-H.; Isaeva, A.; Müller, U.; Schnelle, W.; Simon, P.; Doert, T.; Ruck, M. *Inorg. Chem.* **2012**, *51*, 7370. (g) Fuhr, O.; Dehnen, S.; Fenske, D. *Chem. Soc. Rev.* **2013**, *42*, 1871. (h) Lin, Y. M.; Massa, W.; Dehnen, S. *Chem.—Eur. J.* **2012**, *18*, 13427. (i) Heine, J.; Dehnen, S. *Z. Anorg. Allgem. Chem.* **2012**, *638*, 2425.

(6) Kovnir, K.; Kolen'ko, Y. V.; Baranov, A. I.; Neira, I. S.; Sobolev, A. V.; Yoshimura, M.; Presniakov, I. A.; Shevelkov, A. V. *J. Solid State Chem.* **2009**, *182*, 630.

(7) (a) Bronger, W.; Kyas, A.; Müller, P. *J. Solid State Chem.* **1987**, *70*, 262. (b) Silvestre, J.; Hoffmann, R. *Inorg. Chem.* **1985**, *24*, 4108. (c) Bronger, W.; Genin, H. S.; Müller, P. *Z. Anorg. Allgem. Chem.* **1999**, *625*, 274. (d) Bronger, W. *Angew. Chem., Int. Ed. Engl.* **1981**, *20*, 52. (e) Nissen, H. P.; Nagorny, K. *Z. Physik. Chem.* **1976**, *99*, 209.

(8) (a) Guionneau, P.; Marchivie, M.; Bravic, G.; Létard, J. F.; Chasseau, D. *Top. Curr. Chem.* **2004**, *234*, 97. (b) Phan, H.; Chakraborty, P.; Chen, M.; Calm, Y. M.; Kovnir, K.; Keniley, L. K.; Hoyt, J. M.; Knowles, E. S.; Besnard, C.; Meisel, M. W.; Hauser, A.; Achim, C.; Shatruk, M. *Chem.—Eur. J.* **2012**, *18*, 15805.

(9) (a) Kitagawa, S.; Kitaura, R.; Noro, S. *Angew. Chem., Int. Ed.* **2004**, *43*, 2334. (b) Yaghi, O. M.; O'Keeffe, M.; Ockwig, N. W.; Chae, H. K.; Eddaoudi, M.; Kim, J. *Nature* **2003**, *423*, 705. (c) Rowsell, J. L. C.; Yaghi, O. M. *Microp. Mesopor. Mater.* **2004**, *73*, 3.

(10) (a) *Mössbauer Spectroscopy Applied to Inorganic Chemistry*; Long, G. J., Grandjean, F., Eds.; Plenum Press: New York, 1984, Vol. *1*. (b) Gütlich, P.; Ensling, J. Mössbauer Spectroscopy. *Ullmann's Encyclopedia of Industrial Chemistry*; Wiley-VCH: 2001.

(11) (a) McQueen, T. M.; Huang, Q.; Ksenofontov, V.; Felser, C.; Xu, Q.; Zandbergen, H.; Hor, Y. S.; Allred, J.; Williams, A. J.; Qu, D.; Checkelsky, J.; Ong, N. P.; Cava, R. J. *Phys. Rev. B* **2009**, *79*, 014522. (b) Mizuguchi, Y.; Takano, Y. *J. Phys. Soc. Jpn.* **2010**, *79*, 102001. (c) Wilson, J. A. *J. Phys.: Condens. Matter* **2010**, *22*, 203201.

(12) Brese, N. E.; O'Keeffe, M. *Acta Crystallogr. B* **1991**, *B47*, 192.

(13) Reissner, M.; Steiner, W.; Boller, H. *Hyperfine Interact. C* **2002**, *5*, 197.

(14) Our preliminary measurements (Quantum Design PPMS) of the single crystals of $Fe_3Se_4(en)_2$ along the $FeSe_2$ chain propagation direction indicate the metallic type of the temperature dependence of the resistivity.

(15) Landrum, G. A.; Dronskowski, R. *Angew. Chem., Int. Ed.* **2000**, *39*, 1560.

(16) (a) Sun, L. L.; Chen, X. J.; Guo, J.; Gao, P. W.; Huang, Q. Z.; Wang, H. D.; Fang, M. H.; Chen, X. L.; Chen, G. F.; Wu, Q.; Zhang, C.; Gu, D. C.; Dong, X. L.; Wang, L.; Yang, K.; Li, A. G.; Dai, X.; Mao, H. K.; Zhao, Z. X. *Nature* **2012**, *483*, 67. (b) Medvedev, S.; McQueen, T. M.; Troyan, I. A.; Palasyuk, T.; Eremets, M. I.; Cava, R. J.; Naghavi, S.; Casper, F.; Ksenofontov, V.; Wortmann, G.; Felser, C. *Nat. Mater.* **2009**, *8*, 630.